PERGAMON

International Journal of Heat and Mass Transfer 41 (1998) 2909–2924

International Journal of HEAT and MASS TRANSFER

Boiling vertical two-phase flow at sub-atmospheric pressures

Henrik Kockum,* Åke Jernqvist

Department of Chemical Engineering 1, Lund University, P.O. Box 124, SE-221 00 Lund, Sweden

Received 25 September 1997; in final form 22 December 1997

Abstract

An experimental set-up for the measurement of steady-state two-phase flow data at sub-atmospheric pressures has been built. It has been used to provide data for boiling water. Void fraction data showed a distinct mass quality dependence but only a weak mass flux dependence. Friction pressure drop was calculated from the measured total pressure drop. A clear dependence was found on mass quality and on mass flux. Quasi-local heat transfer coefficients were calculated from temperature and heat flow measurements. Nucleate boiling was found to dominate the heat transfer, although the convective contribution was evident. Empirical correlations for all the quantities were derived.

Key words: Sub-atmospheric pressure; Boiling; Vertical; Two-phase; Heat pumps.

Nomenclature

A area [m^2]
Bo boiling number [—]
D diameter [m]
f one-phase friction factor [—]
g acceleration due to gravity [$m\ s^{-2}$]
h specific enthalpy [$J\ kg^{-1}$]
k overall heat transfer coefficient [$W\ (m^{-2}\ K^{-1})$]
p absolute pressure [Pa]
P perimeter [m]
q heat flow rate [W]
Re Reynolds number [—]
T temperature [K]
w mass flow rate [$kg\ s^{-1}$]
y general parameter [—]
Y general quantity [—]
z axial coordinate [m].

Greek symbols

α heat transfer coefficient [$W\ (m^{-2}\ K^{-1})$]
δY uncertainty of general quantity [—]
Δ difference operator [—]
ε void fraction [—]
E_b bias limit (root of square-sum of systematic errors) [—]
E_p process limit (root of square-sum of random errors) [—]
ε_b general systematic error [—]
ε_p general random error [—]
λ thermal conductivity [$W\ (m^{-1}\ K^{-1})$]
μ dynamic viscosity [Pa s]
ρ mass density [$kg\ m^{-3}$]
σ standard deviation [—]
Φ friction pressure gradient multiplier [—]
χ mass quality [—]
X Lockhart–Martinelli parameter [—]
Ψ heat transfer coefficient multiplier [—].

Subscripts

a acceleration
amb evaluated in the ambient
b evaluated for bulk of flow
c evaluated at core of flow
f friction
g gravitation
ins evaluated in the insulation of the heated wall
l liquid
lo two-phase flow is considered as liquid only
loss loss
lv evaporation
v vapour
tb tube material
tt turbulent–turbulent (in Lockhart–Martinelli parameter)

* Corresponding author.

0017–9310/98 $19.00
PII: S0017-9310(98)00020-9

w evaluated at inside of wall
wo evaluated at outside of wall.

Superscripts
a″ per unit area [m^{-2}]
ã denotes error that arises from common error source [—].

1. Introduction

The technology of industrial energy conservation includes, among other means, the use of heat pumps. Two common types of heat pumps are mechanical heat pumps and absorption heat cycles. The latter can be further divided into absorption heat pumps and absorption heat transformers (AHTs). An AHT may be constructed so as the necessary pressure differences of its components are maintained by hydrostatic legs. In such an AHT it is possible to circulate the working medium pair without electrical pumps, and has been termed a self-circulating AHT [1, 2]. A newer type of AHT which also is self-circulating is a multi-compartment AHT for different steam qualities (a MAD transformer) [3–5]. Transportation of the working medium pair from the absorber (working at the higher pressure) to the generator (working at the lower pressure) is achieved using a thermosiphon arrangement. The flow from the absorber is depressurised by throttling and flashes. The generated vapour entrains the liquid and transports it to the generator vessel. The purpose of the generator is to evaporate some of the refrigerant (the volatile component) and thus, regenerate the solution at the lower pressure, part of which is achieved in the tube. For the working medium pair, water vapour and aqueous sodium hydroxide solution, the suitable absolute pressures for the absorber and the generator are about 100 and 10 kPa, respectively [2]. A temperature lift from 90–130°C is then possible. The present paper is part of a project in which the thermosiphon is studied.

In order to design the thermosiphon arrangement in self-circulating AHTs and MADs using one-dimensional separated two-phase flow models, one will need expressions for the heat transfer coefficient, friction pressure drop, and the void fraction. Boiling vertical two-phase flow in general is indeed an area well covered in research, both in the context of evaporators and steam generators. However, most studies have been done on boiling systems at higher pressures, e.g. steam generators in the power industry, or for refrigeration cycles with different types of fluorocarbons normally working at super-atmospheric pressures. Since most correlations have been derived from higher pressure experiments, a low pressure experimental set-up was built to obtain pertinent experimental data in order to compare to existing correlations, and, if necessary, derive new correlations. This paper reports about the experimental set-up, the results of the experiments done with boiling water flows at sub-atmospheric pressures, and the correlations of the data. Future work will include measurements with binary mixtures with one non-volatile component.

The objective of the boiling water runs presented in the present work was to obtain an understanding of the thermosiphon process in the absence of, primarily, mass transfer resistance which will be present when binary mixtures are studied. Furthermore, the water results are suitable to be used as references for the future binary mixture runs. In a recent work, Cheah [6] studied the (total) pressure drop and heat transfer characteristics of convectively evaporating water in a vertical tube with mass fluxes ranging from 50–350 kg ($m^{-2} s^{-1}$), heat fluxes from 10–50 kW m^{-2}, and absolute exit pressures from 25–100 kPa. In an extensive literature survey [6], Cheah found only one work which had a close relation to his work, viz. that of Stone [7], who used mass fluxes ranging from 0.7–140 kg ($m^{-2} s^{-1}$), heat fluxes between 44 and 11 400 kW m^{-2}, and absolute exit pressures between 24 and 690 kPa [6]. In the present work, void fraction and friction pressure drop were, in addition to heat transfer characteristics, studied at mass fluxes ranging from 70–300 kg ($m^{-2} s^{-1}$), heat fluxes from 0–13.5 kW m^{-2}, and absolute pressures between 8 and 55 kPa.

2. Experimental work

2.1. Experimental set-up

The general layout of the set-up is shown in Fig. 1, where key positions are marked with circled numbers (0–3). A mass flow rate controlled centrifugal pump circulates the fluid which is pumped from an open storage tank to a steam-heated plate heat exchanger. The fluid temperature after the heater is controlled. If the steam pressure is throttled to a sub-atmospheric pressure the vacuum pump is used, otherwise the condensate is discharged through a steam trap. After the fluid has been heated it is flashed in a manually controlled valve at position 0, flows upwards in a 27.3 mm inner diameter tube to the measurement section and the void meter, and then to the liquid–vapour separator. The liquid is cooled in a heat exchanger before it is returned to the storage tank, while the vapour is condensed and withdrawn with a vacuum pump. From positions 1–2 the vertical distance is 0.900 m, and from positions 2–3 it is 1.700 m. The vertical distance from positions 0–1 was alternated between 5.785 and 0.810 m.

The electrically heated measurement section is used to obtain data for heat transfer coefficient and friction pressure drop evaluation. The pipe (27.3 mm inner diameter industrial quality stainless steel tube, SS2343) was heated using heating foils (electrically heated sheets) with

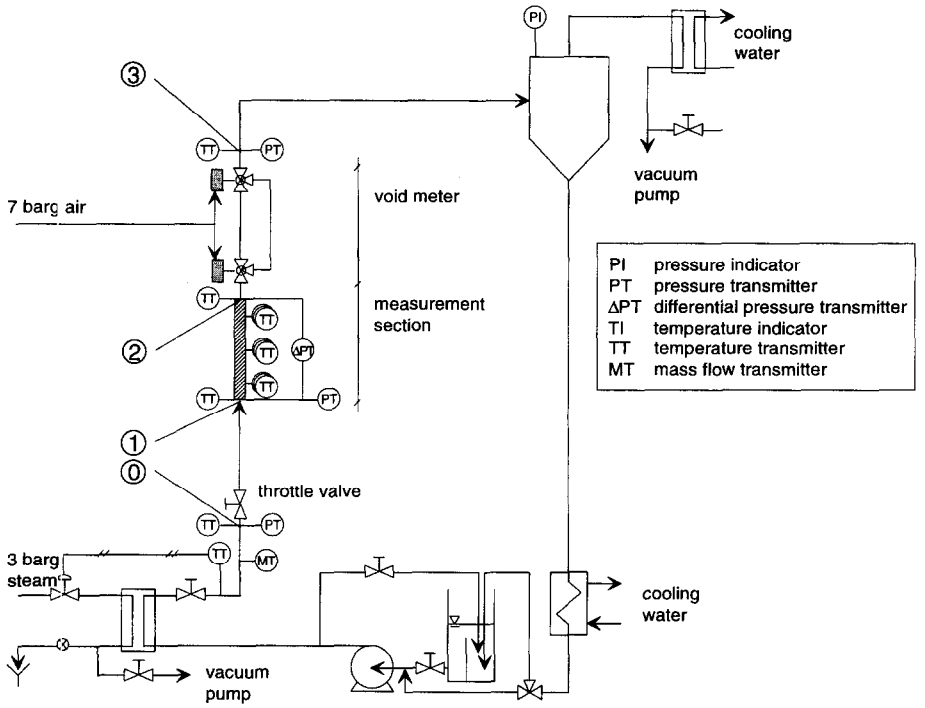

Fig. 1. Schematic flowsheet of the experimental set-up; circled numbers are position numbers.

a total maximum power of 2000 W. The power to the foils was varied using a variable AC-transformer. The heated section was 0.866 m long resulting in a maximum heat flux of about 27 000 W m^{-2}. The wall temperature was measured at three circumferential positions at three axial positions, totalling nine positions with type T thermocouples (TCTs). The 0.5 mm diameter TCTs were placed in 0.25 mm deep axially running grooves on the tube surface. Four layers of copper band (10 mm wide, 0.1 mm thick) were wound between the heating foils and the tube in order to even out any effects of uneven heating of the heating foils. Together with the bands thermal conduction paste mixed with fine aluminium powder was used. Outside the foils glass-fibre ropes (approximately 7 mm in diameter) were wound tightly to ensure good contact between the foils and the copper. Outside the ropes a rolled aluminium sheet (1 mm thick) was attached using hose clamps to apply even more pressure on the heating foils. All this was then dressed in 50 mm insulation with an aluminium shell.

2.2. Instrumentation

The core temperature of the fluid was measured by four resistance temperature measuring devices of type Pt100 (RTDs) at positions 0–3. These were inserted at a 45° angle to the flow. The absolute pressure was measured at positions 0, 1, and 3, as well as the pressure difference between positions 1 and 2. The total mass flow rate was measured before position 0 with a Coriolis force flow meter (Krohne Corimass MFS 2200), calibrated by the manufacturer. At one position, on the inside of the thermal insulation of the measurement section, the temperature was sampled with a TCT and the ambient temperature was read using a thermometer.

The void meter consisted of two full-bore three-way ball valves, a main tube (a vacuum-insulated glass tube with inner diameter 23.8 mm) where the liquid hold-up was read, and a stainless steel by-pass tube in which the fluid flowed when the main tube was closed for reading. The ball valves could be closed simultaneously using pneumatic actuators controlled by solenoid valves. The closing-time was estimated to 0.2 s. Before reading the hold-up the liquid was allowed to drain for approximately 20 s, but no further steps were taken to correct for wall wetting. Reading of the hold-up scale was done at the liquid level in order to minimise the parallax error.

Visual observations of the flow pattern were done in the void meter.

The vertical tube arrangement was thermally insulated from the mass flow meter up to a point 0.4 m beyond position 3.

The TCTs and the RTDs were calibrated to an accuracy of 0.1 K (including errors stemming from the data

acquisition system) using a reference RTD (Pt100) with an uncertainty of 0.01 K. Absolute (Endress and Hauser Cerabar PMC 133) and difference pressure transducers (Fuji Electric FCX) were calibrated by the respective manufacturer. Estimated bias limits of the instruments are shown in Table 1.

All transducers were logged every two seconds using a 12-bit AD-converter and stored on a PC for further treatment. Electric power and liquid hold-up readings were done manually at 30 and 90 s intervals, respectively. The ambient temperature was read only once for each run.

2.3. Experimental procedure

Before starting an experimental series, the water was recirculated while heated and exposed to low pressure in order to be degassed. During this procedure, which lasted for about an hour, the instrumentation was also warmed-up.

Each experimental run was performed at constant condenser settings (cooling water flow rate and air leakage opening), mass flow rate, pre-heating, and throttle-valve setting (position 0 in Fig. 1). A constant condenser setting will give an approximately constant exit pressure. The wall heat flux was varied at four values, including an adiabatic condition. Thus, four different values of friction pressure drop (one adiabatic and three diabatic), three values of heat transfer coefficient, and one value of void fraction were obtained from each run. Each run lasted about 40 min.

A total of 43 runs were made over the parameter ranges specified in Table 2. Twelve of these runs were made with the throttle valve close to the measurement section (0.810 m) in order to obtain lower qualities than was possible with the throttle valve further away (5.785 m) from the measurement section.

Table 1
Estimated bias limits of measured quantities

Quantity	Estimated bias	Comment
Temperature	0.1 K	Both TCTs and RTDs
Absolute pressure	0.55%	Of maximum
Difference pressure	1%	Of maximum
Mass flow rate	5%	If $w_l < 0.025$ kg s^{-1}
	0.5%	If $w_l < 0.05$ kg s^{-1}
	0.3%	If $w_l < 0.1$ kg s^{-1}
	0.2%	Otherwise
		Of reading
Electric power	1%	Of reading

Table 2
Values of key parameters

Parameter	Values	Units
w''^{a}	70, 104, 171, 255	kg (m^{-2} s^{-1})
w''^{b}	92, 136, 225, 336	kg (m^{-2} s^{-1})
q''^{a}	3500, 7900, 13 500	W m^{-2}
$p_b{}^{a}$	12.4–54.3	kPa
$p_b{}^{b}$	7.6–36.1	kPa
χ^{a}	0.0035–0.086	—
χ^{b}	0.011–0.106	—

[a]Measurement section.
[b]Void meter.

2.4. Validation of set-up

One phase flow measurements were performed in order to validate the set-up. Heat transfer coefficients agreed within experimental error to the ESDU correlation [8], and the friction factor agreed with accepted values [9], including a relative wall roughness of 0.0011–0.0018 for the tube used [10].

A check on the energy balance over the heated measurement section was also done for one-phase flows. A bulk average temperature had to be calculated for the exit temperature (position 2 in Fig. 1). At first this was calculated according to the theoretical relationship between the bulk and the wall temperatures at constant wall heat flux and fully developed turbulence (e.g. [11]), viz.

$$\frac{T_b - T_w}{T_c - T_w} = \frac{5}{6}, \tag{1}$$

Using this relationship an outflow of energy significantly larger than the inflow was obtained. However, using values of 0.90–0.95 instead of $\frac{5}{6} \approx 0.83$ it was possible to balance the energy. This higher value implies a more plug-like temperature profile, which could be the result of a higher degree of turbulence, originating from the temperature probe upstream (RTD at position 1) and a pipe coupling about 0.5 m upstream of the RTD at position 1. Furthermore, heat conduction along the RTD probe at position 2, as well as the fact that the heated zone ended 17 mm upstream of position 2, may result in calculated bulk average temperatures that were too high. The exact cause of the imbalanced energy was not pursued, but the authors were content with that the imbalance could be explained.

Void fractions were measured for two-phase air–water flows at near atmospheric pressure and agreed quite well with data obtained by Anderson and Mantzouranis [12]. The friction pressure gradient multiplier for the air–water measurements was found to agree within experimental

error (which was, on the average, 20%) with the Lockhart and Martinelli multiplier [13].

3. Data reduction

From each run four sections were chosen to form the base for the following calculations. Hence, the 43 runs resulted in 172 sub-runs. Each sub-run represented at least 100 s (normally 150 s) of data sampling, implying at least 51 (normally 76) values for each measured quantity. The heating power and the liquid hold-up are data which were not logged automatically. The heating power was read ten times over 5 min for each setting, and the liquid hold-up was read 11 times over 15 min for each void fraction point. With these series of data, time-averages and standard deviations of the measured quantities were calculated and processed further as described in the following.

The fluid state (p, T, χ) was determined at positions 0–3. The average state of the measurement section and the void meter were calculated using the arithmetic mean of the states at positions 1 and 2, and 2 and 3, respectively. When determining the thermodynamic state for a two-phase mixture the temperatures were used to calculate the pressure assuming equilibrium conditions. For a measured temperature and its total uncertainty one can calculate the uncertainty in the equilibrium pressure using the slope of the vapour pressure curve. Likewise, the uncertainty of the equilibrium temperature due to experimental uncertainty in the pressure may be estimated. By comparing calculated and experimental uncertainties one can decide which quantity is the more accurate. The measured core temperatures were taken as average temperatures, thus assuming that the flow is completely mixed.

The quality at a certain position was calculated assuming thermodynamic equilibrium and using the energy balance for separated two-phase flow in difference form as follows:

$$0 = \Delta\{w''A[(1-\chi)h_l+\chi h_v]\} + \frac{1}{2}\Delta\left\{w''^3A\left[\frac{(1-\chi)^3}{\rho_l^2(1-\varepsilon)^2}+\frac{\chi^3}{\rho_v^2\varepsilon^2}\right]\right\} + (w''A\boldsymbol{g}-q''_wP_w)\Delta z+q_{loss} \quad (2)$$

where the Δ is the difference operator with respect to the axial coordinate. At position 0 the fluid is subcooled and thus, has a known vapour content (zero). The heat loss term q_{loss} was evaluated for the measurement section as described below, while for the other parts it was taken as zero since the temperature is higher there due to the electrical heating.

The heat loss was evaluated using

$$q_{loss} = (kA)_{loss}(T_{ins}-T_{amb}) \quad (3)$$

where the temperature difference was measured between the inside of the insulation and the ambient. $(kA)_{loss}$ was determined by isolating the measurement section and, at steady conditions, note the heat input and the temperature difference. $(kA)_{loss}$ was noted to remain practically constant at a value of 0.5 W K^{-1}. This value was therefore used when estimating the heat loss for each sub-run, although it could have been ignored, being in the range 10–30 W where the higher value corresponds to higher heat inputs. Thus, the relative heat losses, compared to the heat inputs, were approximately 5%.

The void fraction was calculated using the measured liquid hold-up as the volume fraction of the closed void meter that the vapour phase occupied.

The friction pressure drop was evaluated using

$$\frac{\Delta p_f}{\Delta z} = \frac{\Delta p}{\Delta z} - \frac{\Delta p_g}{\Delta z} - \frac{\Delta p_a}{\Delta z} \quad (4)$$

where $\Delta p/\Delta z$ was obtained experimentally and

$$\frac{\Delta p_g}{\Delta z} = -\rho\boldsymbol{g} = -[(1-\varepsilon)\rho_l+\varepsilon\rho_v]\boldsymbol{g} \quad (5)$$

$$\frac{\Delta p_a}{\Delta z} = -w''^2\Delta\left[\frac{(1-\chi)^2}{\rho_l(1-\varepsilon)}+\frac{\chi^2}{\rho_v\varepsilon}\right] \quad (6)$$

where the densities were evaluated at average bulk temperature and pressure, T_b and p_b, respectively, and the void fraction was calculated from a suitable expression, given below.

The quasi-local heat transfer coefficient was calculated (and defined) by

$$\alpha = \frac{q''_w}{T_w-T_b} \quad (7)$$

where the heat flux is referred to the inside wall area of the tube, and

$$T_b = \tfrac{1}{2}(T_{c,1}+T_{c,2}) \quad (8)$$

where subscripts 1 and 2 refer to positions 1 and 2 in Fig. 1. The inside wall temperature was evaluated as

$$T_w = T_{wo} - \frac{q''_w}{2\lambda_{tb}}D_w\ln\frac{D_{wo}}{D_w} \quad (9)$$

where the average outside wall temperature was taken as the arithmetic average of the nine TCTs in the measurement section, or

$$T_{wo} = \frac{1}{9}\sum_{j=1}^{9}T_{wo,j}. \quad (10)$$

When calculating the heat flux to the fluid the heat losses from the measurement section were taken into account.

3.1. Analysis of experimental uncertainty

To estimate the propagated uncertainty at a 95% confidence level for the calculated quantities the random errors ε_p, which control the precision limit, and the sys-

tematic errors ε_b, which control the bias limit, were used in the computerised data reduction. The time-averaged value of each measured parameter was sequentially perturbed to obtain its effect on the calculated quantity. The essence of the sequential perturbation scheme was suggested and described by Moffat [14, 15].

The methodology to estimate the propagated uncertainty in a calculated quantity is described in standard text books on statistics and error analysis, e.g. Taylor [16]. Consider an arbitrary calculated quantity y which depends on m measurable parameters y_j,

$$Y = Y(y_j), \quad j = 1, 2, \ldots, m. \tag{11}$$

The propagated uncertainty in Y, δY, may then be written

$$\delta Y = \sqrt{E_p^2 + E_b^2}. \tag{12}$$

Here the precision limit is (if all $\varepsilon_{p,j}$ are independent)

$$E_p^2 = \sum_j \left(\frac{\partial Y}{\partial y_j}\varepsilon_{p,j}\right)^2 \tag{13}$$

and the bias limit is

$$E_b^2 = \sum_j \left(\frac{\partial Y}{\partial y_j}\varepsilon_{b,j}\right)^2 + \sum_j \sum_{k \neq j} \frac{\partial Y}{\partial y_j}\frac{\partial Y}{\partial y_k}\tilde{\varepsilon}_{b,j}\tilde{\varepsilon}_{b,k} \tag{14}$$

where the double-sum is taken over those parameters which have identical systematic error sources such as the calibration means and procedures, implying the errors are in total correlation, and $\tilde{\varepsilon}_b$ denotes the portions of the systematic errors that arise from those identical sources.

The magnitude of the random errors were estimated from the standard deviation. For a 95% confidence level $\varepsilon_{p,j} = 2.0\sigma_j$ if at least 30 values were used, as the case was for most of the parameters, when obtaining the time-averaged value. In the case of electric power and liquid hold-up readings only 10 or 11 values were used, respectively, then $\varepsilon_{p,j} = 2.2\sigma_j$. Systematic errors arise from several sources and are more difficult to quantify. In the present analysis both the calibration error and the calibration curve fitting error are included. Furthermore, errors in physical property data were taken into account; they were set to 1% for all properties, except surface tension which was ascribed an uncertainty of 2%. The partial derivatives appearing in equations (13) and (14) were evaluated numerically.

4. Results and discussions

Based on the values of key parameters given in Table 2, the ranges and approximate relative uncertainties of key quantities were calculated and the results are displayed in Table 3. Since the uncertainties generally vary with each experiment, approximate relative precision and bias limits, and total uncertainties of some calculated quantities are also shown in Table 3.

Observed flow patterns were plug/churn, churn, churn/annular, and annular flows. A few qualitative statements can be mentioned about the flow pattern observations: the transition, expressed in the reciprocal Lockhart–Martinelli parameter

$$\frac{1}{X_{tt}} = \left(\frac{\chi}{1-\chi}\right)^{0.9}\left(\frac{\rho_l}{\rho_v}\right)^{0.5}\left(\frac{\mu_v}{\mu_l}\right)^{01} \tag{15}$$

from churn to annular flow decreased as total mass flux w'' increased; plug/churn flow was observed only for the lowest w''; churn flow was not observed for the highest w''.

4.1. Void fraction

The measured void fractions are shown in Fig. 2. It should be mentioned that the pressure varies for the different points. Apart from the expected dependence of the void fraction on the quality, a dependence, although rather weak and not possible to justify on statistical grounds, on mass flux was also noted. The void fraction has been replotted in Fig. 3 using the inverse Lockhart–Martinelli parameter $1/X_{tt}$, thus, taking into account the varying pressure, and the Reynolds number, based on the total flow,

$$Re_{lo} = \frac{w'' D_w}{\mu_l} \tag{16}$$

as parameters where this dependence becomes somewhat clearer. The void fraction tended to increase with Re_{lo} when plotted against $1/X_{tt}$, which is also what would be expected. Since the average pressure in the void meter was not held constant it is difficult to isolate the pressure effect on the void fraction. However, most of the effect of pressure should have been taken into account by using the inverse Lockhart–Martinelli parameter instead of the mass quality χ.

In the void fraction case the precision limit is largely determined by the type of flow pattern and not only by random variations in the process. If one were to monitor the void fraction at a certain axial position and as a function of time, one could count the number of occurrences of a certain void fraction (or, rather, an interval) and then plot the probability of observing this void fraction (interval), see e.g. Rouhani and Sohal [17]. A plug flow void fraction would, in such a plot, show two peaks, one at low and one at high void fractions, a result of the alternating passing of liquid plugs and vapour bubbles. The standard deviation for the time averaged void fraction in plug flow will therefore be relatively large. Annular flow, then, would generate only one peak (at high void fraction). In the present work the void fraction was measured using the closing-valve technique, and so the time varying local void fraction cannot be monitored. However, closing the valves in plug flow will result in the 'catching' of a number of plugs. The number will vary from closing to closing, and thus, in a way, reflect the

Table 3
Ranges and approximate relative uncertainties of calculated key quantities

Quantity	Range	Units	E_p/Y	E_b/Y	$\delta Y/Y$	No. of points
ε^b	0.781–0.966	—	0.15	0.004	0.15	43
$\Phi_{lo}^{2\,a}$	−159–432	—	0.30	0.12	0.32	172
$\Psi_{lo}{}^a$	1.33–6.59	—	0.11	0.06	0.13	129
α^a	2710–5720	W (m^{-2} K^{-1})	0.11	0.07	0.13	129
$Bo \cdot 10^{6a}$	5–75	—	0.02	0.03	0.03	129
$Re_{lo}{}^a$	3550–20 680	—	0.02	0.02	0.03	172
$Re_{lo}{}^b$	3440–20 740	—	0.02	0.01	0.03	43
$1/X_{tt}{}^a$	0.28–6.91	—	0.02	0.01	0.03	172
$1/X_{tt}{}^b$	0.89–10.22	—	0.02	0.01	0.02	43

[a]Measurement section.
[b]Void meter.

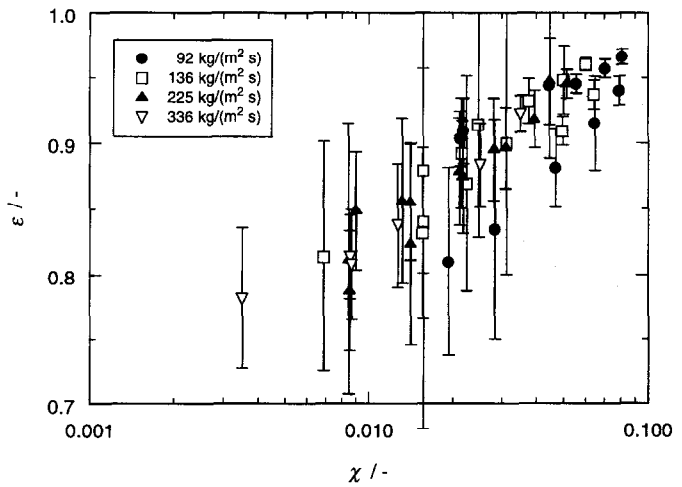

Fig. 2. Measured void fraction as a function of quality with mass flux as parameter; the error bars reaching outside the graph are for points where only one measurement was made, subsequently the uncertainty is infinite.

intermittent nature of plug flow. Hence, one should expect larger standard deviations for plug, or churn, flow than for annular flow.

One more source of uncertainty, which was not accounted for, in the void fraction measurements is the systematic error (although one may imagine it is dependent on, e.g., the mass flow rate) introduced with a non-instantaneous closing of the valves, resulting in a disturbance of the flow and flow pattern.

The experimental void fraction data were compared to some existing models and correlations, viz. the homogeneous void fraction, the Lockhart and Martinelli [13] correlation (in the popular form due to Chisholm [18]), equation (7) of Zivi [19], Premoli et al. [20], and the model of Huq and Loth [21], see Fig. 4 and Table 4. Both the homogeneous model and the correlation of Premoli et al. grossly overpredict the experimental void fraction data, showing that there is a considerable average phase velocity difference. The Lockhart and Martinelli correlation was found to agree very well with the present experimental data. The rather simple Zivi model, which has been used in the analysis of pressure drop data [22], predicted data quite well, although it tended to overpredict. The Huq and Loth equation overpredicted the void fraction and with a tendency to larger deviations at lower void fractions; most of the data in the present range, however, had a relative deviation of less than 10%.

The following empirical equation correlated the experimental data quite well, and is included in Fig. 4,

$$\varepsilon = \frac{1}{1+4.82(X_{tt}^{0.526}-0.477X_{tt}^{0.263})Re_{lo}^{-0.227}}. \quad (17)$$

Note that the turbulent–turbulent Lockhart–Martinelli parameter was used irrespective of what the Reynolds

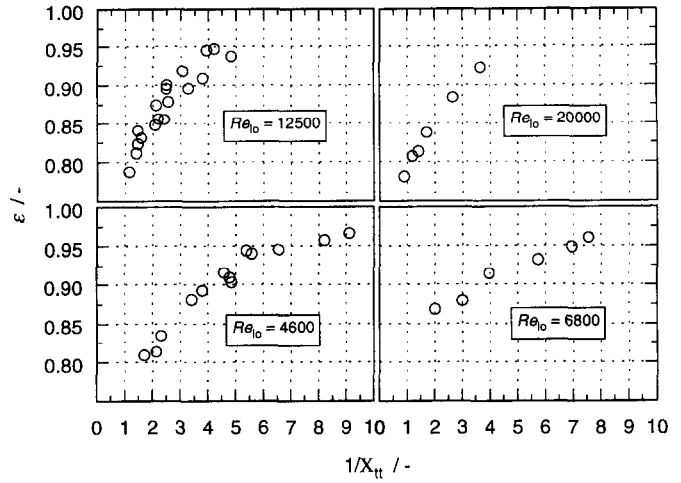

Fig. 3. Measured void fraction as a function of the inverse Lockhart–Martinelli parameter with the Reynolds number as parameter.

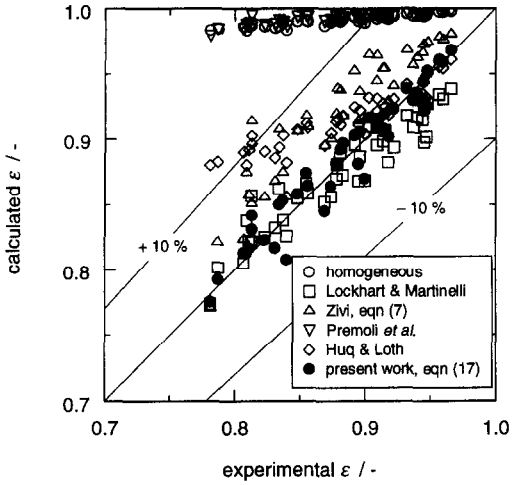

Fig. 4. Parity plot of experimental and calculated void fractions.

number based on the liquid phase flowing alone in the pipe, Re_l, actually was.

4.2. Friction pressure gradient

The void fraction is needed to evaluate the friction pressure gradient according to equations (4)–(6). The equation fitted to the present void fraction data, equation (17), and the Lockhart and Martinelli correlation [13, 18] were used in the data reduction. It should be noted that an extrapolation of equation (17) was necessary for $1/X_{tt} < 0.9$ in the reduction of data.

Using equation (17) a few data points (4 of 172) at lower qualities ($0.015 < \chi < 0.02$) and with the observed flow pattern of plug/churn flow showed a positive friction pressure gradient as can be seen in Fig. 5 which includes all friction data (diabatic and adiabatic). A positive friction pressure gradient is not physically impossible since the wall shear stress changes direction more or less periodically for plug and churn flows, and the time-averaged shear stress on the wall may be directed downwards [23]. Data at low qualities are scattered for the mass fluxes 104 and 255 kg (m^{-2} s^{-1}). As can be seen in Fig. 5, it is evident that the friction pressure gradient depends, at least, on the quality and the mass flux. If friction data are expressed instead as a two-phase multiplier,

$$\Phi_{lo}^2 = \frac{\dfrac{dp_f}{dz}}{\dfrac{dp_{f,lo}}{dz}} \tag{18}$$

and plotted as a function of $1/X_{tt}$ the mass flux, or Reynolds number, dependence remains although not as distinct (see Fig. 6 which contains both diabatic and adiabatic data). The scatter of the data for a mass flux of 104 kg (m^{-2} s^{-1}) does not seem to correlate to different flow patterns as churn flow was observed for all points (plug/churn for one point) at $1/X_{tt} < 2$, although it is admitted that differences in flow pattern may be difficult to observe with the naked eye. The four data points at $1/X_{tt} < 1$ are the only part of the data set where a definite influence of the wall heat flux was found. For these points the two-phase multiplier Φ_{lo}^2 increases with the heat flux q''. However, one should not draw any general conclusions about the heat flux dependence with such few data.

Reducing the pressure drop data using the void correlation of Lockhart and Martinelli [13, 18] yields friction pressure gradients with three points having positive values, although very close to zero. Studying the cor-

Table 4
Correlations and models used in the comparisons

Quantity	Correlation/model	Equation
ε	Homogeneous	$\varepsilon = \dfrac{1}{1+\dfrac{1-\chi}{\chi}\dfrac{\rho_v}{\rho_l}}$
	Lockhart and Martinelli [13, 18]	$\varepsilon = 1-\dfrac{1}{\left(1+\dfrac{20}{X_{tt}}+\dfrac{1}{X_{tt}^2}\right)^{0.5}}$
	Zivi, equation (7) [19]	$\varepsilon = \dfrac{1}{1+\dfrac{1-\chi}{\chi}\left(\dfrac{\rho_v}{\rho_l}\right)^{2/3}}$
	Premoli et al. [20]	$\varepsilon = \dfrac{1}{1+S\dfrac{1-\chi}{\chi}\dfrac{\rho_v}{\rho_l}}$
		$S = 1+E_1\left(\dfrac{y}{1-yE_2}-yE_2\right)^{0.5}$
		$y = \dfrac{\beta}{1-\beta}$
		$\beta = \dfrac{1}{1+\dfrac{1-\chi}{\chi}\dfrac{\rho_v}{\rho_l}}$
		$E_1 = 1.578 Re_{lo}^{-0.19}\left(\dfrac{\rho_v}{\rho_l}\right)^{0.22}$
		$E_2 = 0.0273 We_{lo}\, Re_{lo}^{-0.51}\left(\dfrac{\rho_v}{\rho_l}\right)^{-0.08}$
	Huq and Loth [21]	$\varepsilon = 1-\dfrac{2(1-\chi)^2}{1-2\chi+A}$
		$A = \left[1+2B\left(\dfrac{\rho_l}{\rho_v}-1\right)\right]^{0.5}$
		$B = 2\chi(1-\chi)$
Φ_{lo}^2	Lockhart and Martinelli [13, 18]	$\Phi_{lo}^2 = (1-\chi)^{1.8}\cdot\left(1+\dfrac{20}{X_{tt}}+\dfrac{1}{X_{tt}^2}\right)$
	Chisholm [24]	$\Phi_{lo}^2 = 1+(\Gamma^2-1)[B\chi^{0.9}(1-\chi)^{0.9}+\chi^{1.8}]$
		$\Gamma = \dfrac{\rho_l}{\rho_v}\left(\dfrac{\mu_v}{\mu_l}\right)^{0.2}$
		$B = \dfrac{15\,000}{\Gamma^2 w''^2}$ since $\Gamma \geqslant 28$ for all data

(Continued overleaf)

Table 4
Continued

Quantity	Correlation/model	Equation
	Friedel [25]	$\Phi_{lo}^2 = E + \frac{3.24FH}{\left(\frac{w''^2}{gD_w\rho^2}\right)^{0.045}\left(\frac{w''^2 D_w}{\rho\sigma}\right)^{0.035}}$
		$E = (1-\chi)^2 + \chi^2 \frac{\rho_l f_{vo}}{\rho_v f_{lo}}$
		$F = \chi^{0.78}(1-\chi)^{0.24}$
		$H = \left(\frac{\rho_l}{\rho_v}\right)^{0.91}\left(\frac{\mu_v}{\mu_l}\right)^{0.19}\left(1-\frac{\mu_v}{\mu_l}\right)^{0.7}$
		$\rho = \left(\frac{\chi}{\rho_v} + \frac{1-\chi}{\rho_l}\right)^{-1}$
Ψ_{lo}	Schrock and Grossman [27]	$\Psi_{lo} = 7.39\left(Bo\cdot 10^3 + \frac{0.15}{X_{tt}^{2/3}}\right)$
	Pujol and Stenning [28]	$\Psi_{lo} = 9.0\left(Bo\cdot 10^3 + \frac{0.445}{X_{tt}^{0.37}}\right)$
	Mayinger and Ahrens [29]	$\Psi_{lo} = 8.5\left(Bo\cdot 10^3 + \frac{0.45}{X_{tt}^{0.35}}\right)\left(1+\frac{D_w}{L_{hw}}\right)^{\frac{1}{X_{tt}^{0.41}}}$

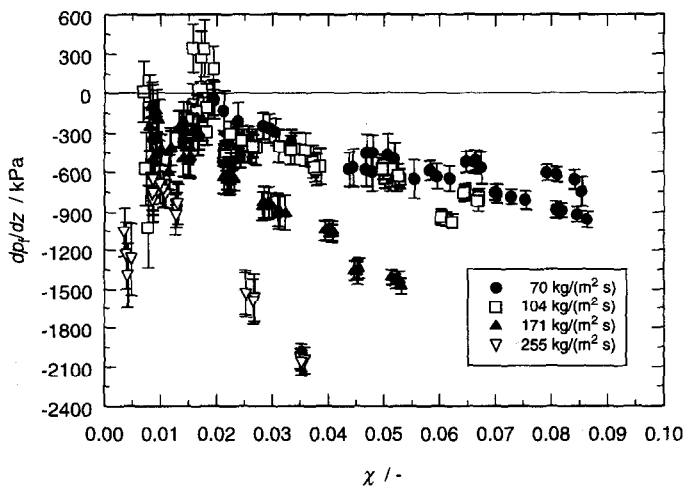

Fig. 5. Friction pressure gradient evaluated using equation (17); the uncertainty in the abscissa was of the order of 0.001.

responding Φ_{lo}^2 in Fig. 7 one observes that the mass flux dependence remains but the inverse Lockhart–Martinelli parameter dependence is less pronounced.

Comparisons of the Φ_{lo}^2, obtained in the present work using equation (17), and the correlations of Lockhart and Martinelli [13], Chisholm [24], and Friedel [25] are shown in Fig. 8. Note that the negative multipliers are not shown. The correlations are listed in Table 4.

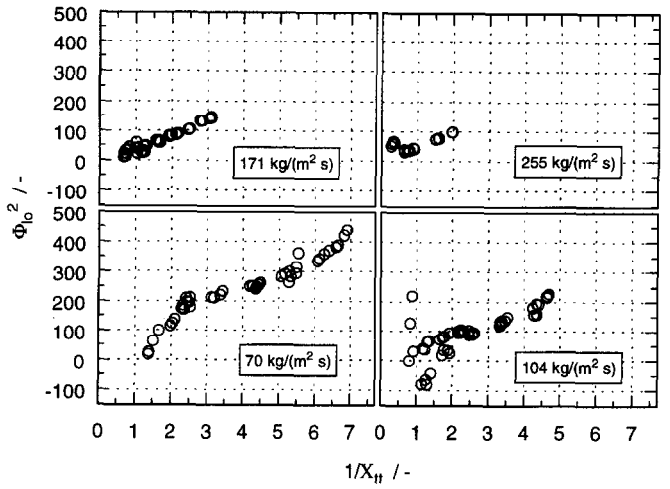

Fig. 6. Two-phase flow multiplier, evaluated using equation (17), as a function of the inverse Lockhart–Martinelli parameter with the total mass flux as parameter; the uncertainty in the abscissa was of the order of 0.1.

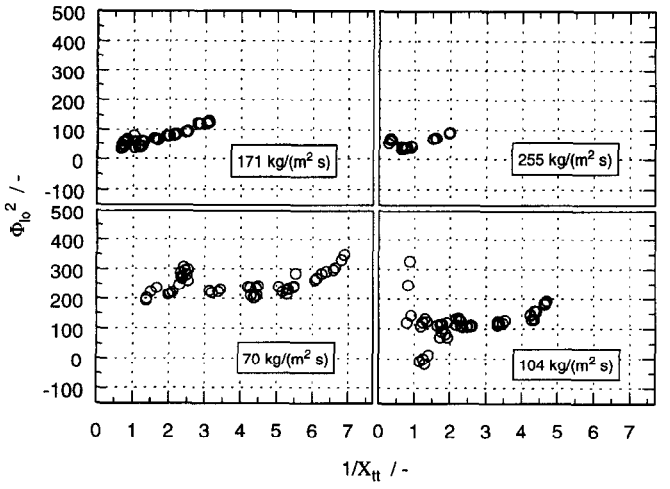

Fig. 7. Two-phase flow multiplier, evaluated using the correlation of Lockhart and Martinelli [13, 18], as a function of the inverse Lockhart–Martinelli parameter with the total mass flux as parameter; the uncertainty in the abscissa was of the order of 0.1.

The multiplier of Lockhart and Martinelli is defined as

$$\Phi_l^2 = \frac{\dfrac{dp_f}{dz}}{\dfrac{dp_{f,l}}{dz}}. \tag{19}$$

There is, however, a quite straightforward relationship between this definition and the definition used in the present work, viz.

$$\Phi_{lo}^2 = (1-\chi)^{2-n}\Phi_l^2 \tag{20}$$

where n is the exponent of the Reynolds number in the Blasius expression for the one-phase friction factor,

$$f = \frac{const}{Re^n}. \tag{21}$$

The original Lockhart and Martinelli multiplier, in the form set by Chisholm [18], was thus recalculated according to equation (20) in order to be used in the comparison. From Fig. 8 it can be seen that both the Lockhart and Martinelli and the Chisholm correlations predict the multiplier quite well although they both tend to underestimate it. The Friedel correlation, on the other hand, grossly overpredicts Φ_{lo}^2.

If Φ_{lo}^2 was calculated using the void correlation of Lockhart and Martinelli, the Lockhart and Martinelli

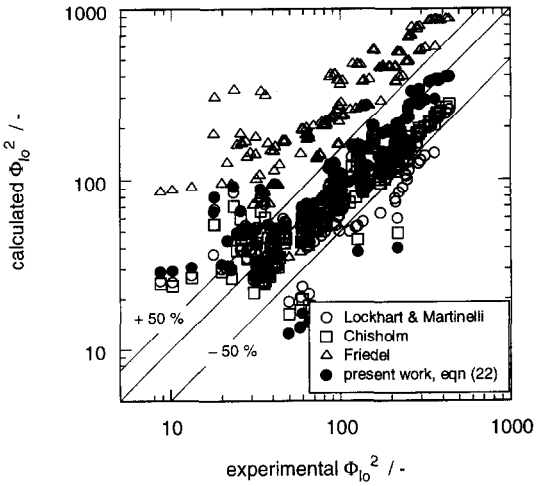

Fig. 8. Parity plot of experimental and calculated friction pressure gradient multipliers; note that the negative multipliers are not shown.

and Chisholm correlations improved somewhat for low values of Φ_{lo}^2, while growing worse at higher ones. The overall scatter increased somewhat.

It was difficult to obtain a good fit of the present data due to the unexplained scatter at low $1/X_{tt}$. The following expression fitted the data reasonably well, except for low $1/X_{tt}$,

$$\Phi_{lo}^2 = \left(1 + \frac{41.4}{X_{tt}} - \frac{2.48}{X_{tt}^2}\right)\left(1 + \frac{16\,990}{X_{tt}\, Re_{lo}^{1.364}}\right). \tag{22}$$

This expression is included in Fig. 8.

4.3. Heat transfer

The heat transfer coefficient α for a mass flux of 104 kg (m^{-2} s^{-1}) is plotted as a function of χ and with the heat flux as a parameter in Fig. 9. One notes that it depends both on the heat flux and the mass quality, although rather weakly on the latter. In Fig. 10 α has been plotted for all mass fluxes, showing an increasing dependence on χ as the mass flux increases, although further influence of the mass flux seems to be absent. It is interesting to note the spread in the heat transfer coefficient α at $\chi \approx 0.015$ for the mass flux 104 kg (m^{-2} s^{-1}) and the heat flux 3500 W m^{-2} in Figs. 9 and 10. The point with the highest α is one of the points that showed a positive friction pressure gradient. However, no further connections to the scattered data in Fig. 6 seem to exist, except that all flows were plug/churn or churn flows. It is not impossible that there is an influence of flow pattern or flow pattern transitions in this region of the data.

Since, in effect, it was the separator pressure that was controlled in the experiments the pressure at a given point will vary from run to run although the separator pressure was the same. An attempt to elucidate the effect of pressure has been done in Fig. 11 where some of the 70 kg (m^{-2} s^{-1}) data have been plotted. However, from Fig. 11 and Table 3 it is evident that no specific conclusions about the effect of pressure could be drawn. A clear heat flux dependence and a rather weak quality dependence as well as a limited mass flux dependence suggest that the heat transfer was dominated by nucleate boiling. For pure nucleate boiling one would expect the heat transfer coefficient to increase with pressure, while, for a given χ, velocities are expected to decrease, thereby decreasing α, with increasing pressure. Clearly, the situation is complex. Cheah [6] found his heat transfer experiments to be nucleate boiling dominated at mass qualities above 0.05. Cheah further noted that no clear-cut causes could be identified to the pressure dependence of the heat transfer coefficient, owing to the complexity. One may also note that Kenning and Hewitt [26] observed that the heat flux where nucleate boiling starts to dominate decreases with decreasing mass quality and decreasing mass flux. They obtained heat transfer coefficients for boiling vertical flow of water at mass fluxes of 123, 203, and 304 kg (m^{-2} s^{-1}) and qualities of -0.1–0.7 at nominal pressures of 160 and 390 kPa. The heat transfer data, obtained with a cupronickel tube and heat fluxes of 50–400 kW m^{-2}, included both nucleate and convection dominated boiling. Heat transfer coefficients ranging from 6 to 40 kW (m^{-2} K^{-1}) were obtained.

The heat transfer coefficients of the present work were also evaluated as two-phase multipliers, defined by

$$\Psi_{lo} = \frac{\alpha}{\alpha_{lo}} \tag{23}$$

using the ESDU correlation [8] for the single phase heat transfer coefficient, α_{lo}. Figure 12 shows the multipliers dependence on the inverse Lockhart–Martinelli parameter, which is expected to eliminate the pressure dependence, mass flux, and heat flux. Qualitatively, there is little that differs from the heat transfer coefficient as plotted in Fig. 10. However, with increasing mass flux Ψ_{lo} decreases.

A temperature difference between the wall and fluid bulk which differed from zero was measured even when no heat was supplied. Analysis of the data revealed that it was a result of the continuous flashing of the flow. The thermal inertia of the wall prevented its temperature following that of the bulk of fluid more closely than it did.

The multiplier was then compared to the correlations of Schrock and Grossman [27], Pujol and Stenning [28], and Mayinger and Ahrens [29] in Fig. 13. The correlations of Mayinger and Ahrens and Pujol and Stenning both overpredict Ψ_{lo}, while that of Schrock and Grossman tends to underpredict it. Since the comparing correlations were not produced for the present conditions the deviations are not surprising.

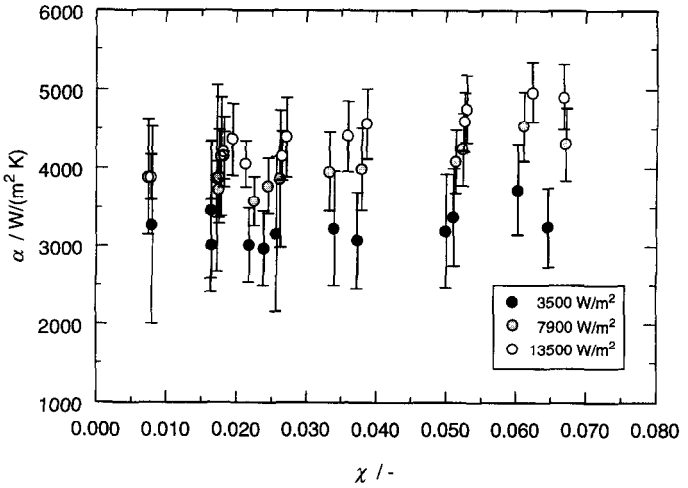

Fig. 9. Heat transfer coefficient at a mass flux of 104 kg (m^{-2} s^{-1}).

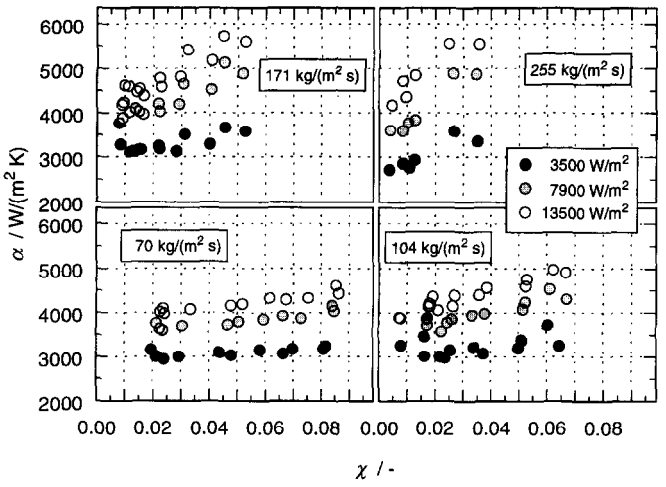

Fig. 10. Heat transfer coefficient dependence on quality, mass flux, and heat flux.

Following Schrock and Grossman [27], a simple correlation based on the Lockhart–Martinelli parameter and the boiling number *Bo*, defined by

$$Bo = \frac{q''}{w'' h_{lv}} \tag{24}$$

was sought, not implying that these two parameters are the only ones pertinent to the problem, but is rather a reflection of the scope of the investigation. In any case, *Bo* is a representation of the nucleate boiling contribution, while the $1/X_{tt}$ is a representation of the convective contribution. It was possible to correlate the data to within 50% with the following equation

$$\Psi_{lo} = 46\left(Bo \cdot 10^3 + \frac{0.041}{X_{tt}^{0.34}}\right) \tag{25}$$

which has been included in Fig. 13. One may note that the first coefficient on the right hand side of equation (25), 46, is an order of magnitude larger than the corresponding coefficients of the other correlations, thus, enhancing the nucleate boiling contribution while the convective boiling contribution is still of the same order of magnitude as in the other correlations.

5. Conclusions

In order to provide experimental information for the design of the thermosiphon in self-circulating AHTs and MADs, an experimental set-up for the measurement of steady-state void fraction, pressure drop, and heat trans-

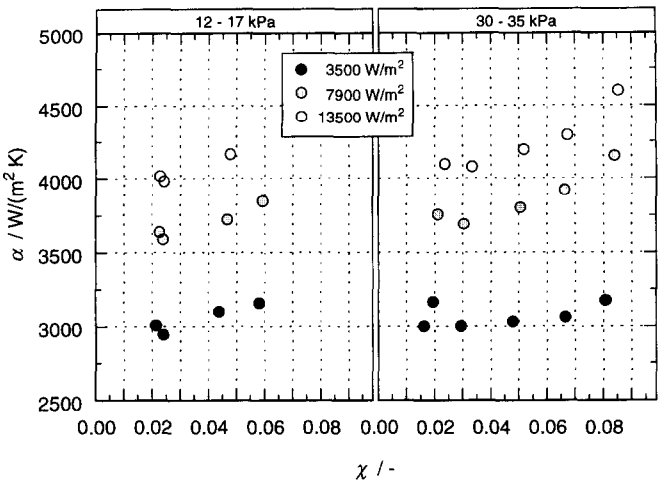

Fig. 11. Heat transfer coefficient at two different pressures for a mass flux of 70 kg ($m^{-2} s^{-1}$).

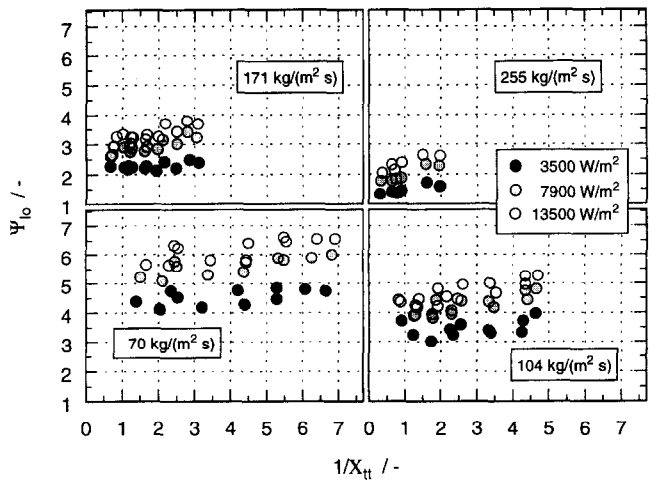

Fig. 12. Heat transfer coefficient multiplier dependence on the inverse Lockhart–Martinelli parameter, mass flux, and heat flux.

fer data for two-phase flows at sub-atmospheric pressures has been built and validated. It has then been used to obtain data for boiling water. These data serve the purposes of providing a basic understanding of the low pressure thermosiphon process, and as references to future measurements of binary mixtures.

Void fractions were measured using the closing-valve technique. The measured void fraction data showed expected characteristics: it increased with the inverse Lockhart–Martinelli parameter $1/X_{tt}$ and, although rather weakly, with the Reynolds number Re_{lo}. The flow could not be modelled with the simple homogeneous model as was evident from the void fraction data. It seems possible, however, to use the Lockhart and Martinelli correlation [13, 18] with confidence, although a correlation representing data better could be produced, equation (17).

The friction pressure drop was calculated from the measured total pressure drop. These data included a few points with a positive friction pressure drop, all in connection with plug/churn flow. A clear dependence of the friction pressure drop was found on both mass quality χ and mass flux w''. Of the existing friction pressure gradient multipliers used in the present work best agreement was found with the expression given by Chisholm [24].

A quasi-local heat transfer coefficient was calculated from temperature measurements over a 0.9 m section of the tube. Nucleate boiling was found to be the dominating heat transfer mechanism although the convective contribution was evident. A significant influence of the

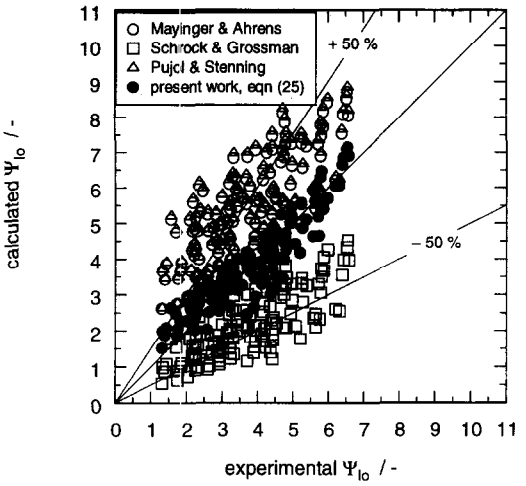

Fig. 13. Parity plot of experimental and calculated heat transfer coefficient multipliers.

pressure on the heat transfer coefficient could not be found. None of the existing simple heat transfer coefficient multipliers utilised in the present work predicted the experimental values well. It was possible, however, to correlate Ψ_{lo} with a simple expression containing *Bo* and $1/X_{tt}$ with maximum deviation of 50%, equation (25).

There was some unexplained scatter in the two-phase multipliers Φ_{lo}^2 and Ψ_{lo} at low $1/X_{tt}$ for the mass flux 104 kg $(m^{-2}\,s^{-1})$.

It should not come as a surprise that most correlations used in the comparisons do not predict data very well as they were developed at different conditions than in the present work.

Acknowledgements

The authors wish to express their gratitude to Dr Gharib Aly for helpful discussions. The equipment support of Alfa-Laval Thermal and the financial support of the Swedish Research Council for Engineering Sciences are gratefully acknowledged.

References

[1] Eriksson K, Jernqvist Å. Heat transformers with self-circulation: design and preliminary operational data. Int J Refrig 1989;12(1):15–20.
[2] Abrahamsson, K. Absorption heat cycles—an experimental and theoretical study. Ph.D. thesis, Lund, Sweden: Lund University, 1993.
[3] Swedish Patent No. 9 203 775-3.
[4] Jernqvist Å, Aly G. A novel multi-compartment absorption heat transformer for different steam qualities. Proceedings of the First European Congress on Chem Engng, Florence, Italy, 1997;4:3043–6.
[5] Scott M, Jernqvist Å, Olsson J, Aly G. Experimental and theoretical study of an open multi-compartment absorption heat transformer for different steam qualities, Part II: process modelling and simulation. Applied Thermal Engng, 1997, submitted.
[6] Cheah LW. Forced convective evaporation at sub-atmospheric pressure. Ph.D. thesis, London, U.K.: London University, 1995.
[7] Stone JR. Subcooled and net boiling heat transfer to low pressure water in electrically heated tubes. NASA Technical Note TN D-6402, Cleveland Ohio, U.S.A.: Lewis Research Center, 1971.
[8] Hewitt GF, Shires GL, Bott TR. Process Heat Transfer, Chap. 2. Boca Raton, FL, U.S.A.: CRC Press, 1994.
[9] Churchill SW. Friction-factor equation spans all fluid-flow regimes. Chem Engng 1977;84(24):91–2.
[10] Gustafsson B-A. In Alvear C, editor, Pumphandboken, Chap. 2. Göteborg, Sweden: EuroContact Publishers AB, 1979.
[11] Burmeister LC. Convective Heat Transfer, Chap. 11.2. New York, NY, U.S.A.: John Wiley and Sons, 1983.
[12] Anderson GH, Mantzouranis BG. Two-phase (gas/liquid) flow phenomena—II liquid entrainment. Chem Engng Sci 1960;12(4):233–42.
[13] Lockhart RW, Martinelli RC. Proposed correlation of data for isothermal two-phase, two-component flow in pipes. Chem Engng Progr 1949;45(1):38–48.
[14] Moffat RJ. Contributions to the theory of single-sample uncertainty analysis. J Fluids Engng 1982;104:250–60.
[15] Moffat RJ. Using uncertainty analysis in the planning of an experiment. J Fluids Engng 1985;107:173–8.
[16] Taylor JR. An introduction to error analysis. 1st edition, Chaps 3 and 4. Mill Valley, CA, U.S.A.: University Science Books, 1982.
[17] Rouhani SZ, Sohal MS. Two-phase flow patterns: a review of research results. Progr Nuclear Energy 1983;11(3):219–59.
[18] Chisholm D. A theoretical basis for the Lockhart–Martinelli correlation for two-phase flow. Int J Heat Mass Transfer 1967;10:1767–78.
[19] Zivi SM. Estimation of steady-state steam void-fraction by means of the principle of minimum entropy production. J Heat Transfer 1964;86(2):247–52.
[20] Premoli A, di Francesco D, Prina A. Una correlazione adimensionale per la determinazione della densità di miscele bifasiche. La Termotecnica 1971;25(1):17–26.
[21] Huq R, Loth JL. Analytical two-phase flow void prediction method. J Thermophysics 1992;6(1):139–44.
[22] Souza AL, Chato JC, Wattelet JP, Christoffersen BR. Pressure drop during two-phase flow of pure refrigerants and refrigerant-oil mixtures in horizontal smooth tubes. Proceedings of the 29th Nat Heat Transfer Conference. ASME HTD 1993;243:35–41.
[23] Hewitt GF. Course notes in multiphase flow and heat transfer: bases, modelling, and applications. Chap. 5. Zürich, Switzerland: ETH, 1993.
[24] Chisholm D. Pressure gradients due to friction during the

flow of evaporating two-phase mixtures in smooth tubes and channels. Int J Heat Mass Transfer 1973;16:347–58.

[25] Friedel L. Improved friction pressure drop correlations for horizontal and vertical two-phase flow. 3R Int 1979;18(7):485–91.

[26] Kenning DBR, Hewitt GF. Boiling heat transfer in the annular flow regime. Proceedings of the 8th Int Heat Transfer Conference 1986;5:2185–90.

[27] Schrock VE, Grossman LM. Forced convection boiling in tubes. Nucl Sci Engng 1962;12:474–81.

[28] Pujol L, Stenning AH. Effect of flow direction on the boiling heat transfer coefficient in vertical tubes. In: Rhodes E, Scott DS, editors. Cocurrent Gas–Liquid Flow—Proceedings of an International Symposium on Research in Cocurrent Gas–Liquid Flow, Waterloo, Ontario Canada, 1968. New York, NY, U.S.A.: Plenum Press, 1969. pp. 401–53.

[29] Mayinger F, Ahrens KH. Boiling heat transfer in the transition region from bubble flow to annular flow. Seminar in Two-phase Momentum, Heat, and Mass Transfer in Chemical Engineering 1978;2:591–602.